Tr. J. of Earth Sciences
7 (1998) 167–183

Crystallization Processes and Role of Compositional Convection in the Macrolayer Formation in a Small Layered Complex

Bernard PLATEVOET

Laboratoire de Pétrologie-Volcanologie, B.504, Université de Paris-Sud, 91405 Orsay-FRANCE

Received: 21.05.1998

Abstract: The Peloso complex is a 1000m thick gabbroic body composed of two main layered zones (ZA and ZB) that are made up of cyclic macrolayers of olivine gabbro, leucogabbronorite and anorthosite cumulates, and a third zone of unlayered quartz-gabbro (ZC) which may represent a residual liquid. Within a representative macrolayer, cryptic evolution of minerals can not be neglegted, showing that the crystallizing magma batch had a limited volume and was renewed between the formation of two successive macrolayers. The comparison between calculated parental magma density and densities of successive cumulates shows that the residual liquid was probably extracted by compositional convection at the crystallization front, or by intercumulus compositional convection within the cumulate pile. The calculated convective velocity at the bottom of the layer decreased from 30 cm/year to 10 cm/year when the leucogabbronorite crystalized. The minimum value also gives the order for the crystallization velocity of a macrolayer and a time scale for the reservoir activity.

The residual liquid corresponding to the anorthositic top of a macrolayer is denser than the parent liquid. A strongly unstable density gradient therefore existed with the underlying gabbronoritic residual liquid, and the liquid extraction was prior controlled by the intercumulus convection. Liquids moving through the cumulate, may have induced adcumulus growth of plagioclase and resorption of mafic phases, leading to anorthosite formation at the top of the macrolayer.

Mean crystal sizes, calculated trapped liquid fractions and fractionation density of cumulus associations are linked. Crystal size grading in cumulates is not only controlled by the variations in nucleation rate and crystal growth prevailing at the crystallization front. It is also strongly dependent upon variations concerning amounts, compositions and motions of residual liquids. Finally, in this small layered intrusion, the great majority of cumulates are orthocumulates. Restricted amounts of light residual liquid could have been extracted from them and become mixed with the overlying magma batch, resulting in an overall density decrease.

Assuming that the magma reservoir was stratified, the residual magma batch, becoming gravitationally unstable, would be periodically removed. However, the macrolayer could also represent succesive influxes of new magma in the chamber, it is supported by isotopic studies where the R-F.C. (recharge, fractional crystallization) process is also clearly evidenced in this small magmatic chamber.

Küçük Bir Tabakalı Kompleksde Makrotabakalı Formasyonda Kristalleşme Prosesleri ve Konveksiyon Bileşimin Rolü

Özet: Peloso kompleks 1000 m kalınlığında iki anatabakalı zondan (ZA ve ZB) oluşmaktadır. Bunlar tekrarlanmalı makrotabakalı olivin gabro, loko gabro norit ve anortozit kümülatlardan oluşmakta ve tabakasız kuvars gabrolar (ZC) magmanın son ürünü olarak üçüncü bir zon oluşturur. Tipik bir makrotabakada, minerallerin kriptik evrimi gözardı edilse bil, kristalleşen magmanın küçük hacimde olduğu ve diğer iki makrotabakanın oluşumu sırasında yenilenmiş olduğu anlaşılmaktadır. Hesaplanmış ana magmanın yoğunluğu ile birbirini izleyen kümülatların yoğunluğu karşılaştırıldığında, kalıntı eriyiğin ya kristalleşme cephesinde bileşimsel konveksiyondan, ya da kümülatlar içindeki interkümülüs bileşimsel konveksiyonundan ayrılarak oluştuğu sonucuna varılır. Lokogabronoritlerin kristalleşmesi sırasında tabakanın tabanındaki hesaplanmış konveksiyon akımın hızı 30 cm/yıl dan 10 cm/yıl'a kadar düşmektedir. Minimum değer aynı zamanda bir makrotabakanın kristalleşme hızı değeri ve kaynak aktivitesi için bir zaman ölçeği oluşturur.

Bir mikrotabakanın anortositik tabanı ile temsil edilen kalıntı çözeltinin yoğunluğu ana çözeltiden daha yüksektir. Böylece altdaki gabronoritik kalıntı sıvıda kuvvetli duraysız yoğunluk gradyanları bulunur. Böylece sıvı ayrılması öncelikle interkümülüs konveksiyon ile kontrol edilir. Kümülatların arasından hareket eden sıvılar plajiyoklazların adkümülüs büyümelerini sağlar ve mafik fazları soğurarak mikrotabakaların tavanında anortozitleri oluşturur.

Ortalama kirstal boyları, hesaplanmış kapanlanmış sıvı fraksiyonları ve kümülatların ayrışma yoğunlukları birbiri ile bağlantılıdır. Kümülatlardaki kristal boyutu sadece çekirdeklenme oranındaki değişimlerle ve hakim olarak kristalleşme cephesinde gelişen kristal büyümesine bağlı değildir. Tane boyu kalıntı sıvıların miktarındaki değişimlere, bileşimine ve hareketliliğine bağımlıdır. Sonuç olarak bu küçük tabakalı sokulumlardan kümülatların büyük çoğunluğu ortokümülatlardır. Sınırlı miktardaki hafif kalıntı sıvılar bunlardan ayrılarak üstte bulunan magma ile karışarak yoğunluğunun hafifleşmesine neden olmaktadır.

Magma kaynağının tabakalandığı farz edildiğinde, artakalan magma yığını gravitasyonel olarak duyarsız hale gelir ve periyodik olarak hareketlenir. Ancak mikrotabakalar aynı zamanda magma odasında sürekli yeni magma akımlarını temsil etmektedir. Bu olaylar yeniden beslenme ve fraksiyonel kristalleşme olaylarının varlığı bu küçük magma odalarında kanıtlanmıştır.

Introduction

In the last fifteen years, new models have been proposed to explain igneous layering (Campbell, 1978; Maaloe, 1978; McBirney and Noyes, 1979; Irvine, 1980; Irvine et al., 1983) as alternatives to the classical crystal/liquid gravitational segregation process (Wager and Brown, 1968; Irvine, 1974). Fluid mechanics, experiments in aqueous solutions or viscous oils, theoretical approaches and numerical experiments can now give us new insights on formation of cumulate. Crystallization in situ, double diffusive processes and magma stratification, multiple reinjections and mixing, convection currents, stagnant layers, intercumulus convection and other secondary processes are now proposed to explain many observed features in fossil magma reservoirs (e.g. Chen and Turner, 1980; Huppert and Sparks, 1980; Irvine, 1980; Irvine et al., 1983; Raedeke and McCallum, 1983; Jaupart et al., 1984; Tait et al., 1984; Baker and McBirney, 1985; Wilson and Larsen, 1985; Huppert et al., 1986; Marsh, 1989a and 1989b), but there is no simple general model explaining the crystallization history of layered intrusions (see Parsons, 1987 for a review), as magma chambers are complex systems controlled by multiple and inter-dependent physico-chemical factors.

In the present paper the Peloso layered basic complex which is exposed over and area of about 6 km^2 in southwestern Corsica, is described. It intrudes the Hercynian calc-alkaline batholith and probably belongs to the earliest events of the Permo-Triassic post-orogenic to anorogenic magmatism in Corsica (Bonin, 1972, 1980; Vellutini, 1977; Platevoet, 1990). The chilled margins and the base of the complex are not exposed. The layered sequence is composed of two main zones (ZA and ZB), the uppermost (ZB) is laterally and upwardly replaced by and unlayered quartz-gabbro (ZC). ZC is itself partially eroded and cut by monzonitic and granitic intrusions of alkaline affinities (Figure 1).

The petrographical and mineralogical studies (Platevoet, 1985, 1990), carried out on the entire exposed vertical section of the complex, will be briefly outlined. Then the study will focus on a representative sequence of the ZA zone, to explain the formation of the macrolayers and the behaviour of residual liquids.

Stratigraphy, Main Petrographic and Mineralogical Features of the Complex

Stratigraphy

The structural and petrographical features are described according to the terminology for layered intrusion recommended by Irvine (1982, 1987). The 1000m thick exposed sequence of the Peloso complex has been divided into three zones (ZA, ZB and ZC) on the basis of cumulus phases in the gabbros and norites (Figure 2).

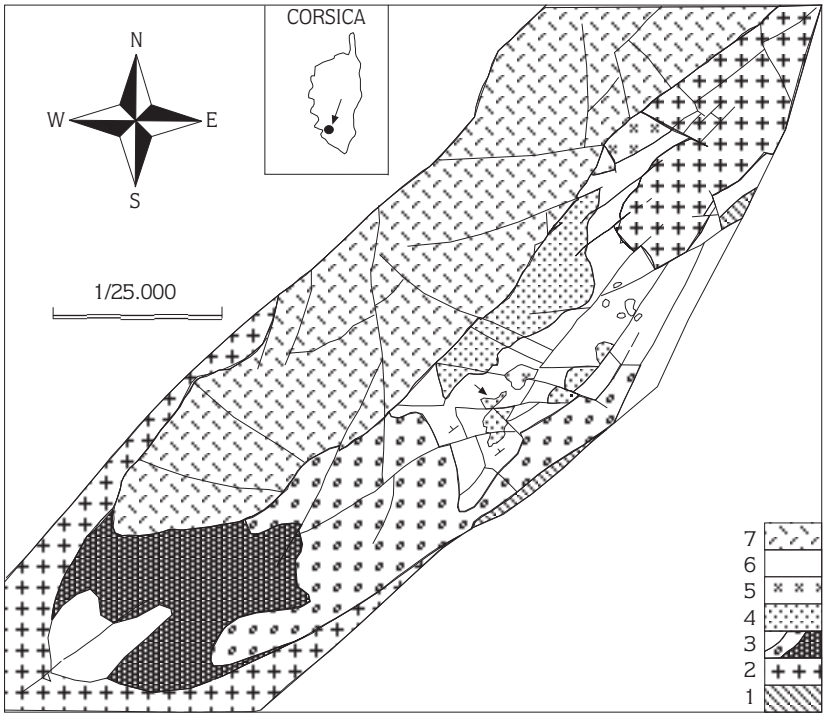

Figure 1. Simplified geological map of the Peloso intrusion. 1: metamorphic basement; 2: calcalkaline granite; 3: ZA zone (ZA1, ZA2, ZA3 from SW to NE); 4: ZB zone; 5: ZC zone (quartz-gabbro); 6: monzonitic intrusion; 7: subsolvus granite.

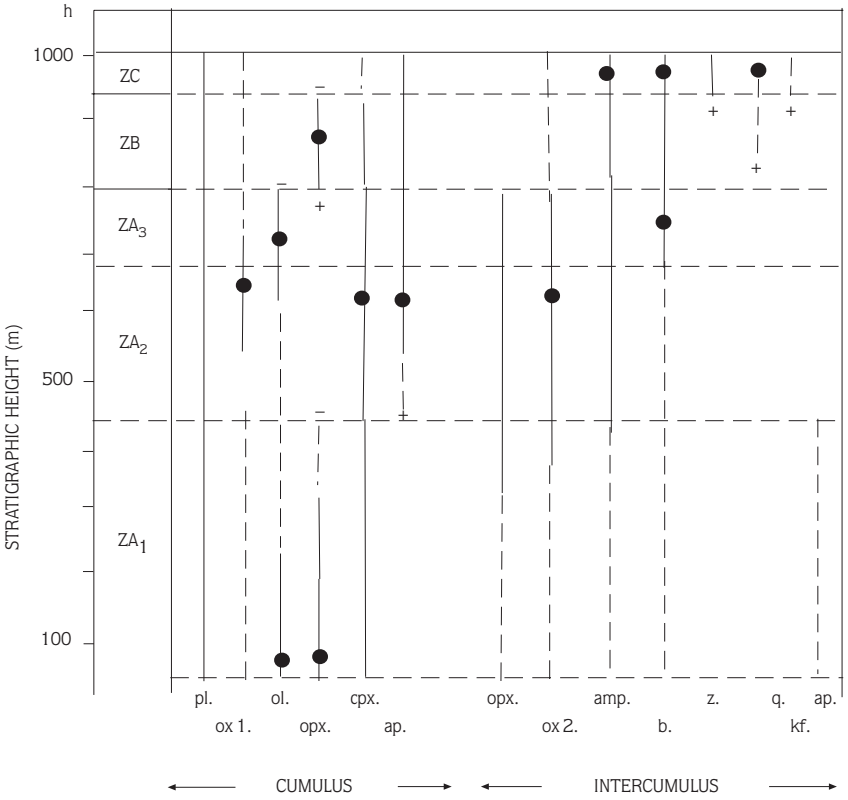

Figure 2. Stratigraphic section through the Peloso intrusion showing the distribution of minerals in gabbros and norites. Pl: plagioclase; ox_1 and ox_2: Fe-Ti oxides (two generations, the second generation consists of poikilitic crystals associated with amphibole); ol: olivine; opx: Ca-poor pyroxene; cpx: Ca-rich pyroxene; ap: apatite; amp: amphibole; b: biotite; z: zircon; q:quartz; kf:K-felspar. Thick, thin or dashed lines: decreasing abundance of phases; dots: for the maximum. The cumulus or intercumulus status of the phases are defined by textural habit.

The lowermost zone (ZA, 700m thick) is defined by the presence of olivine in addition to cumulus plagioclase, Ca-rich pyroxene and Fe-Ti oxide. ZA is further divided into three subzones: ZA1, on the basis of the presence of cumulus Ca-poor pyroxene, ZA2 where cumulus Ca-poor pyroxene is absent and cumulus apatite is present, and ZA3 where apatite and titanomagnetite crystallize as cumulus phases before Ca-rich pyroxene, and where intercumulus biotite is abundant.

The overlying zone ZB (180m thick) contains cumulus Ca-poor pyroxene and no olivine, while the uppermost exposed zone ZC (50m thick) contains minor amounts of Fe-Ti oxide and Ca-rich pyroxene, with abundant subhedral amphibole and zircon.

Intercumulus phases also show systematic variations with stratigraphical height. In the olivine gabbros from the ZA2 and ZA3 subzones, Ca-poor pyroxene occurs as poikilitic crystals enclosing plagioclase, Ca-rich pyroxene and oxide. Amphibole and biotite occur as oikocrysts about 5 mm to 20mm in diameter in all gabbros and norites from ZA and ZB. The ZC gabbro is rich in quartz and has minor interstitial K-feldspar.

In ZA1, modal layering is marked by alternating dm thick macrolayers of leucogabbronorite with anorthositic lenses and thinner melanocratic layers of olivine gabbronorite. Modal grading is commonly developed within the macrolayers, the proportion of plagioclase to mafics increasing upwards. Size-grading also occurs, the crystal-size of plagioclase and pyroxenes increasing from gabbronorite to leucogabbronorite.

ZA2 and ZA3, which are generally better exposed than ZA1, consist of a series of cyclic macrolayers (3m to 20m thick) which can sometimes be traced laterally for 200 to 300m. These macrolayers will be more precisely described in the following section.

The ZB zone has a thickness of only about 180m with no marked structural discontinuity with the ZA zone. Layering is defined by alternating 5m-thick macrolayers of fine-grained norite and and coarser-grained leucogabbro. Within individual macrolayers, modal layering not as well defined as in the ZA zone; however, fine-scale rhytmic layering still occurs especially in leucogabbro macrolayers near the base of the overlying norite layer. Reverse grain-size grading occurs in macrolayers.

The uppermost exposed zone (ZC) is only well exposed in the northern part of the complex; the transition from ZB to ZC is not abrupt the layering and lamination disappearing upwards. ZC is composed

entirely of unlayered quartz-gabbro. Plagioclase is markedly zoned, olivine and orthopyroxene are absent, clinopyroxene is largely replaced by subhedral brown amphibole. Late biotite and quartz are abundant, and there is minor interstitial K-feldspar. Subhedral zircon is common. Mineralogically, the quartz-gabbro is the most evolved rock-type of the complex. The unlayered quartz-gabbro is not interpreted as a cumulate, its bulk composition may be representative of a residual liquid of the chamber.

Mineral Chemistry Evolution Through the Vertical Section

Mineral compositions were determined by electron microprobe analyses of representative rocks. The major variations in mineral chemistry is reported through the entire vertical section of the complex in Figure 3 and Table 1. For simplicity, only the cryptic evolution of major phases in the mafic rock-types (gabbros and norites) is reported.

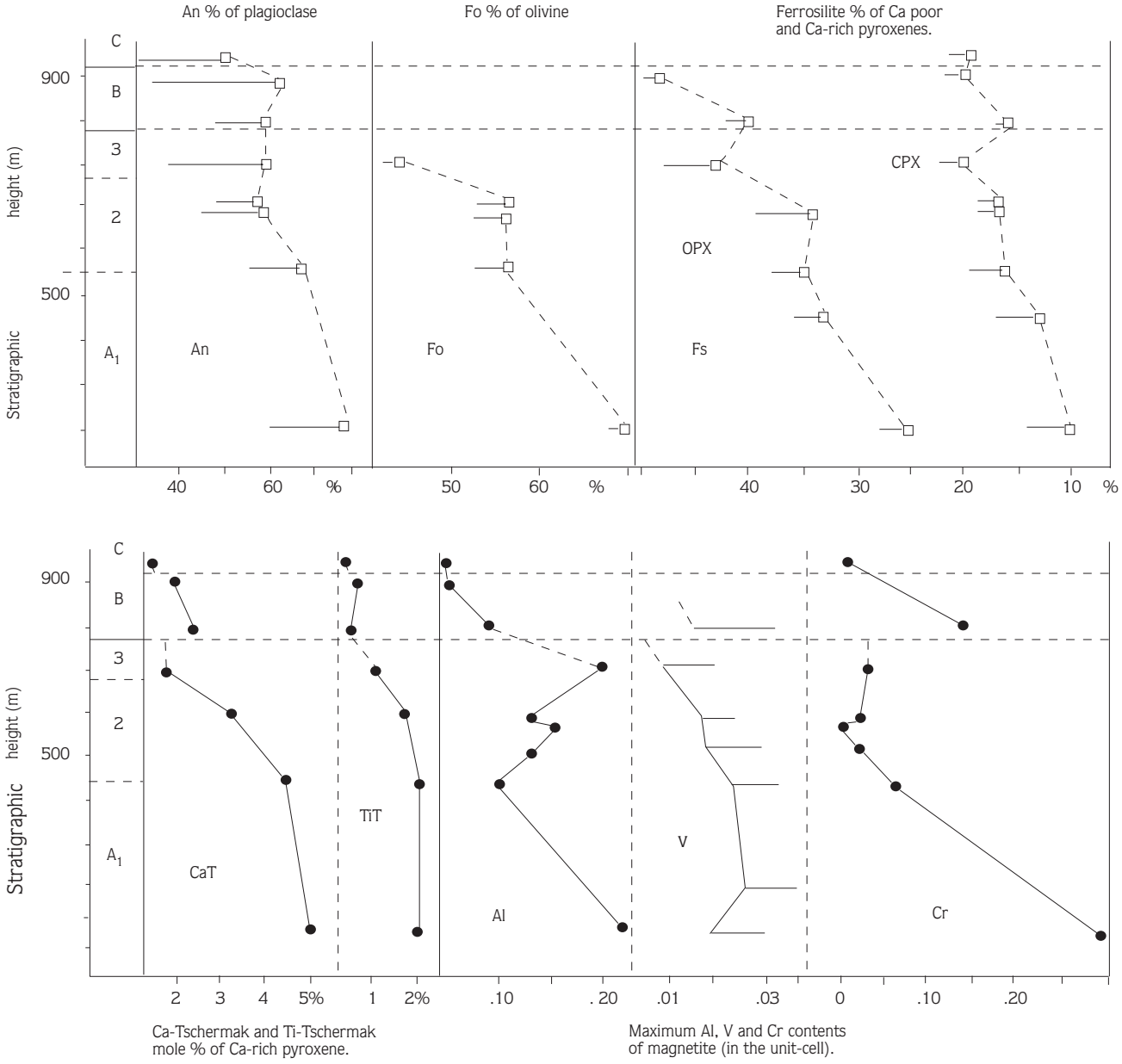

Figure 3. Evolution of mineral composition through the Peloso intrusion. □: composition of crystal cores.

Table 1. Microprobe representative analysis of minerals ir rock examples of the Peloso Complex. CPX: Ca-rich pyroxene. OPX: Ca-poor pyroxene. MGT: magnetite. Plag.: plagioclase. The structural formulas are calculated on the basis of: 6 O fo pyroxenes; 4 O and 3 cations for magnetites; 8 O for plagioclase Rocks are olivine gabbros of ZA, norites of ZB and quartz gabbro o ZC.

rock N°	86083		84089		5-A		84072		84074		84061		85091
mineral	CPX	OPX	CPX	OPX	CPX	OPX	CPX	OPX	CPX	OPX	CPX	OPX	CPX
SiO2	49.96	52.58	51.13	52.99	52.45	53.22	51.38	51.19	51.61	51.28	51.16	50.13	51.62
TiO2	0.76	0.25	0.79	0.23	0.64	0.22	0.45	0.31	0.35	0.18	0.29	0.20	0.27
Al2O3	3.50	1.89	3.24	1.22	2.59	1.26	1.53	0.81	1.84	0.73	1.45	0.60	0.94
Fe2O3	4.70	3.42	1.83	0.77	0.31	0.48	2.85	1.55	3.55	2.84	3.69	2.92	4.10
FeO	2.96	14.53	8.14	20.43	9.68	22.54	11.09	24.80	6.65	21.87	8.85	26.53	7.15
MnO	0.28	0.52	0.00	0.94	0.40	0.75	0.00	0.88	0.34	0.62	0.46	1.23	0.91
MgO	14.48	25.96	13.68	22.73	13.64	22.25	12.54	18.77	13.81	21.22	12.74	17.39	12.50
NiO													
Cr2O3	0.19	0.00	0.00	0.09	0.00	0.03	0.00	0.00	0.11	0.03	0.00	0.00	0.04
V2O5													
CaO	22.97	1.06	21.41	1.31	21.22	0.69	20.76	1.76	22.48	0.84	21.48	1.06	22.40
Na2O	0.42	0.09	0.41	0.00	0.37	0.00	0.39	0.02	0.35	0.02	0.41	0.00	0.63
K2O													
Total	100.22	100.30	100.63	100.71	101.30	101.44	101.00	100.19	101.09	99.62	100.53	100.06	100.57
Si	1.85	1.91	1.90	1.95	1.94	1.96	1.93	1.95	1.91	1.94	1.92	1.94	1.94
Ti	0.02	0.01	0.02	0.01	0.02	0.01	0.01	0.01	0.01	0.01	0.01	0.01	0.01
Al	0.15	0.08	0.14	0.05	0.11	0.05	0.07	0.04	0.08	0.03	0.06	0.03	0.04
Fe3	0.13	0.09	0.05	0.02	0.01	0.01	0.08	0.04		0.08	0.10	0.08	0.12
Fe2	0.09	0.44	0.25	0.63	0.30	0.69	0.35	0.79	0.10	0.69	0.28	0.86	0.22
Mh	0.01	0.02	0.00	0.03	0.01	0.02	0.00	0.03	0.21	0.02	0.01	0.04	0.03
Mg	0.80	1.40	0.75	1.25	0.75	1.22	0.70	1.06	0.76	1.20	0.71	1.00	0.70
Ni													
Cr	0.01	0.00	0.00	0.00	0.00	0.00	0.00	0.00	0.00	0.00	0.00	0.00	0.00
V													
Ca	0.91	0.04	0.85	0.05	0.84	0.03	0.83	0.07	0.89	0.03	0.86	0.04	0.90
Na	0.03	0.01	0.03	0.00	0.04	0.00	0.03	0.01	0.02	0.00	0.03	0.00	0.05
K													

rock N°	86083	84089	5-A	84072	84074	85091
mineral	MGT	MGT	MGT	MGT	MGT	MGT
SiO2	0.06	0.12	0.15	0.18	0.12	0.00
TiO2	8.80	0.79	13.83	19.84	6.61	0.40
Al2O3	5.15	0.56	3.57	2.75	1.93	0.06
Fe2O3	35.19	59.67	34.38	24.77	48.02	68.87
FeO	37.89	33.48	43.15	51.22	37.27	31.58
MnO	0.76	0.00	0.65	0.00	0.00	0.18
MgO	0.86	0.15	0.75	0.00	0.27	0.00
NiO	0.00	0.00	0.00	0.00	0.00	0.00
Cr2O3	9.38	2.32	0.81	0.54	2.36	0.06
V2O5	0.44	1.34	0.74	0.85	0.99	nd
ZnO	0.34	0.00	0.00	0.00	0.26	nd
CaO	0.28	0.00	0.39	0.28	0.60	nd
Na2O						
Total	99.40	98.43	98.42	100.72	98.68	101.15
Si	0.00	0.00	0.00	0.01	0.00	0.00
Ti	0.24	0.02	0.39	0.55	0.19	0.01
Al	0.22	0.03	0.16	0.12	0.09	0.00
Fe3	0.98	1.74	0.97	0.69	1.38	1.97
Fe2	1.19	1.09	1.35	1.58	1.19	1.00
Mn	0.02	0.00	0.02	0.00	0.00	0.01
Mg	0.05	0.01	0.04	0.00	0.01	0.00
Ni	0.00	0.00	0.00	0.00	0.00	0.00
Cr	0.27	0.07	0.02	0.02	0.07	0.00
V	0.01	0.03	0.02	0.02	0.02	nd
Zn	0.01	0.00	0.00	0.00	0.01	nd
Ca	0.00	0.00	0.01	0.01	0.02	0.00
Na						

zone	ZA1	ZA2	ZA2	ZA3	ZA1	ZA2	ZA2	ZA3	ZB	ZB	ZC
rock N°	86083	84089	5-A	84072	86083	84089	5-A	84072	84074	84061	85091
mineral	olivine	olivine	olivine	olivine	plag.	plag.	plag.	plag.	plag.	plag.	plag.
SiO2	37.04	34.81	35.76	33.51	48.59	49.03	54.14	51.96	52.92	51.86	55.96
TiO2	0.07	0.00	0.15	0.09							
Al2O3					32.33	31.05	29.15	29.98	28.96	30.58	27.89
Fe2O3											
FeO	28.21	37.96	38.12	46.67	0.43	0.09	0.13	0.00	0.23	0.24	0.15
MgO	34.72	26.66	26.36	19.11							
MnO	0.53	0.82	0.88	1.15							
NiO	0.01	0.00	0.00	0.00							
Cr2O3											
V2O5											
CaO	0.00	0.00	0.00	0.08	16.48	14.85	11.98	12.67	12.81	13.52	10.69
Na2O					2.41	3.43	4.63	4.36	4.62	3.75	5.48
K2O					0.09	0.24	0.21	0.19	0.24	0.23	0.19
Total	100.58	100.26	101.28	100.61	100.29	98.69	100.24	99.16	99.78	100.18	100.39
Si	0.99	0.98	0.99	0.99	2.22	2.27	2.44	2.38	2.41	2.35	2.51
Ti	0.00	0.00	0.00	0.00							
Al					1.75	1.70	1.55	1.62	1.56	1.64	1.48
Fe3											
Fe2	0.63	0.89	0.89	1.15	0.02	0.00	0.00	0.00	0.01	0.01	0.01
Mh	0.01	0.02	0.02	0.02							
Mg	1.38	1.12	1.09	0.84							
Ni	0.00	0.00	0.00	0.00							
Cr											
V											
Ca	0.00	0.00	0.00	0.00	0.81	0.74	0.58	0.62	0.63	0.66	0.51
Na					0.21	0.31	0.40	0.39	0.41	0.33	0.48
K					0.01	0.01	0.01	0.01	0.01	0.01	0.01

Plagioclase An79, olivine Fo69, Mg-rich pyroxenes and Cr-rich magnetite occur at the bottom of ZA1. Mineral compositions change systematically from bottom to top of the basic complex. From ZA1 to ZA3, the uppermost cumulates are characterized by more albitic plagioclase cores, enrichment in Fe in olivines and pyroxenes, while Ti and Ca-Tschermak components in Ca-rich pyroxene decrease. Within ZA2, pyroxenes display a nearly constant Fe/Mg ratio, in relation to abundant crystallization of Fe-Ti oxides in that subzone. The Cr content of magnetite decreases rapidly with pyroxene fractionation while, the Al content of magnetite first decreases slightly and then increases in ZA2 and ZA3. Similarly, the V content of magnetite reaches a maximum of 0.04 in the unit-cell, in ZA1 and then decreases as a consequence of the probable V-impoverishment of the magma.

The base of ZB corresponds to an abrupt change in the mineral chemistry: pyroxenes again display more primitive compositions. Magnetite becomes enriched in Cr and V, and plagioclase cores are more calcic than in ZA2 and ZA3. The cryptic discontinuity between ZA3 and the base of ZB is in good agreement with modal changes.

In the ZC quartz gabbro, plagioclase becomes more sodic (An51 to An29), and clinopyroxene and amphibole are more Fe-rich than in ZB cumulates. The quartz-gabbro is therefore the most evolved rock-type of the complex.

The Cylic Macrolayers of the ZA2 Subzone

An Example of a Cumulate Sequence

Within the ZA2 subzone, a 100m thick well exposed cumulate sequence has been precisely mapped (Figure 4). The cumulate sequence consists of a series of ten cyclic macrolayers. Contacts between macrolayers are sharp and nearly planar. But the lamination within a macrolayer is often slightly discordant (10° maximum) in relation to the contacts between macrolayers. This interesting feature could be directly dependent upon the process of macrolayer formation itself: crystallization could take place along an inclined accretion front. The contact between the successive macrolayers could depict the

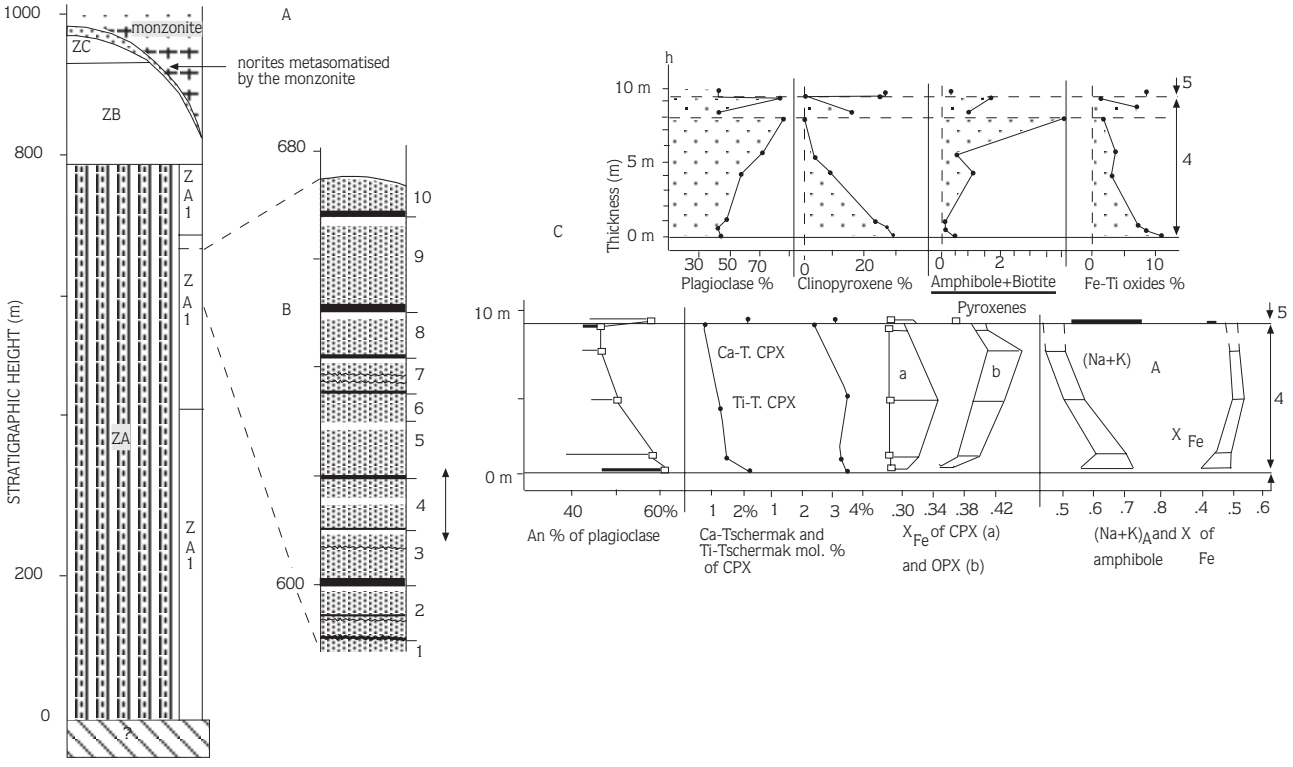

Figure 4. A: Situation of the macrolayer sequence in the ZA2 zone. B: Sequence of ten cyclic macrolayers of ZA2; black layers: olivine gabbro; dashed layers: leucogabbronorite; white layers: anorthosite.
C: Modal and mineralogical variations through the 4th macrolayer: The base of the 5th macrolayer is also plotted. The dashed line is for the base of the reversal. □: composition of mineral cores. X_{Fe} = Fe+Mn/(Fe+Mn+Mg) . $[Na+K]_A$: amphibole [A] site filling.

magma stratification or mark the successive magma influxes in the chamber.

The macrolayer thickness varies from 3 to 10m. The macrolayers display normal modal grading, with the proportion of plagioclase to mafics increasing upwards, and reverse grain-sized grading. A typical 10m thick layer is characterized by fine-grained olivine gabbro at its base, grading rapidly upwards to coarser leucogabbronorite with an anorthositic top. Leucogabbronorite is always the predominant rock-type. The anorthositic top is absent in some macrolayers. However, they may form well defined anorthositic thin layers (2 to 50cm thick) within the dominant leucogabbronorites. Sometimes, evolved pegmatitic pockets are observed under the anorthositic top of some layers and could represent light residual fluids which have been trapped because of the porosity reduction of the anorthositic top.

In the studied sequence, the field proportions of the three rock-types has been approximately determined (9% of olivine gabbro, 74% of leucogabbronorite and 17% of anorthosite), these ratios will be used to calculate a representative mean cumulate of the ZA2 subzone (Table 2).

Modal Grading and Mineral Chemistry of a Representative Macrolayer

A representative macrolayer of the sequence has been chosen for the present study: it is the 4th macrolayer (Figure 4, Table 2), where major modal variations are dominated by plagioclase enrichment toward to top, while conversely, cumulus oxide and clinopyroxene decrease from bottom to top. In leucogabbronorite, olivine is entirely replaced by orthopyroxene crystals which become relatively abundant with respect to

Table 2. A: Chemical analyses. ZA1, ZA2, ZA3, ZB: average compositions of the zones of the Peloso complex; n. rocks: number of rock examples; ZC: average composition of the quartz gabbro assumed to be the last residual liquid (L_f). The 4th macrolayer of ZA2: 4-A, 4-B: olivine gabbros; 4-F: gabbro (basic reversal); 4-C, 4-D: leucogabbronorites; 4-E, 4-G: anorthosites; 5-A: base of the 5th macrolayer.
B: (successive) calculated parental magmas, CIPW norms and physical parameters. L1 to L3: parent magmas for ZA1, ZA2 and ZA3. ZC: last residual liquid. L'2: assumed parent magma at the level of the 4th macrolayer. d: density. μ: viscosity.

A

n. rock	10	17	8	6	5	N°4							N°5
subzones	ZA1	ZA2	ZA3	ZB	ZC	4-A	4-B	4-C	4-D	4-E	4-F	4-G	5-A
thickness	350m	200m	150m	180m	50m	1.00m	1.50m	2.00m	1.5m	2.00m	0.80m	0.20m	1.00m
SiO2	45.56	48.46	50.42	49.07	54.04	45.61	47.18	49.39	46.03	49.87	48.39	52.01	44.71
TiO2	2.8	2.13	1.78	1.73	1.63	2.61	1.78	1.66	2.73	1.69	2.18	1.24	1.81
Al2O3	17.24	19.63	18.01	17.67	16.51	14.31	15.28	18.54	18.85	20.73	15.52	24.68	15.74
Fe2O3						4.21	1.6	3.1	3.13	1.97	6.81	0.86	3.69
FeO	12.31	9.53	9.42	9.58	8.86	11.29	10.23	6.91	7.91	5.91	5.47	3.75	10.24
MgO	5.62	4.4	4.62	5.38	4.5	6.96	7.43	5.12	4.92	2.68	6.01	2.08	6.95
MnO						0.25	0.36	0.19	0.18	0.13	0.21	0.09	0.26
CaO	9.31	9.7	8.08	8.12	6.66	11.92	11.65	10.2	9.92	8.72	9.96	9.01	11.44
Na2O	3.17	3.65	3.72	3.74	3.9	2.08	2.91	3.17	3.52	4.54	3.26	4.84	2.8
K2O	0.77	0.83	1.11	1.34	2.2	0.3	0.48	0.76	0.78	0.83	0.61	0.82	0.42
P2O5	0.49	0.8	0.51	0.53	0.44	0.17	0.31	0.55	0.58	0.9	0.09	0.3	1.14
H2O	1	1.2	1.25	1.4	1.48	0.64	1.62	1.23	1.46	1.15	1.54	1.67	1.37
Total	98.27	100.33	98.92	98.56	100.22	100.35	100.83	100.82	101.01	99.12	100.05	101.35	100.57
Rb	13.6	11.4	15.4	32.8	51	3.4	4.6	12	11	12	8	13	4.8
Ba	191	418	749	348	285	204	265	364	381	498	308	504	301
Sr	394	526	414	329	271	368	391	478	494	661	398	672	431
Ce	23	49	41	85	99.8	14	27	39	81	50	24	31	51
La	nd	nd	nd	nd	nd	15	17	22	38	23	17	15	26
Nd	nd	nd	nd	nd	nd	11	21	26	56	29	24	17	39
Y	18	32	23	47	49	26	33	30	50	20	33	16	44
Zr	149	248	550	706	335	115	161	166	275	98	226	256	154
Nb	7	9	9	16.5	21	2.7	4.6	5.8	12	8.1	7.5	7.8	4.2
Zn	90	84	91	112	107	137	99	98	100	64	108	40	111
Co	39	33	29	31	29.3	61	43	34	37	25	46	14	49
Ni	40	19	33	80	43.5	12	32	25	25	11	6	3	8.5
Sc	40	25	27	25	26	61	50	37	26	3	50	8	39
Cr	57	71	98	109	70.5	179	245	180	2	4	154	13	168
V	416	234	245	160	214	570	273	262	255	122	346	83	377

B

OXYDES	ZC	L.3	L'2	L.2	L
SiO2	54.04	51.23	50.29	49.76	
TiO2	1.63	1.74	1.87	1.94	
Al2O3	16.51	17.67	18.33	18.70	
Fe2O3	1.28	1.38	1.38	1.38	
FeO	8.05	8.70	8.71	8.71	
MnO	0.00	0.00	0.00	0.00	
MgO	4.50	4.59	4.52	4.48	
CaO	6.66	7.76	8.41	8.79	
Na2O	3.90	3.76	3.72	3.70	
K2O	2.20	1.35	1.17	1.07	
P2O5	0.44	0.49	0.59	0.65	
Total	99.21	98.68	99.00	99.19	
Composition normative					
Apatite	0.97	1.08	1.30	1.43	
Ilménite	3.10	3.31	3.56	3.69	
Magnétite	1.86	2.01	2.01	2.01	
Chromite	0.00	0.00	0.00	0.00	
Orthose	13.00	7.98	6.91	6.32	
Albite	33.01	31.82	31.49	31.32	
Anorthite	21.07	27.38	29.89	31.29	
Diopside	7.54	6.58	6.63	6.71	
Orthopyroxène	18.51	13.92	10.01	7.70	
Olivine	0.00	0.00	0.00	0.00	
Néphéline	0.00	0.00	0.00	0.00	
Quartz	0.14	0.00	0.00	0.00	
Total	99.21	98.68	99.00	99.19	
paramètres					
T °C	1100.00	1125.00	1150.00	1150.00	
H2O %	2.00	1.20	1.00	0.75	
d	2.60	2.66	2.68	2.70	
μ Pa.s	74.10	65.90	47.30	51.50	

clinopyroxene. Increasing postcumulus reactions of anhydrous minerals with trapped liquid lead to the development of late poikilitic amphibole, Fe-Ti oxides and biotite. Interstitial hydrous minerals are most abundant at the top of the layer.

The cryptic evolution of minerals (Figure 4, Table 3) in the 4th macrolayer portrays the evolution recorded throughout the ZA2 and ZA3 subzones. Plagioclase cores become more and more sodic upwards, Ca– and Ti-Tschermak components of CPX decrease slightly. Amphibole composition changes from pargasite-hastingsite to hornblende (A-site vacancy becomes >0.5 in the unit-cell) and the Fe/Mg ratio variation follows that of Ca-poor pyroxene with the retrograde evolution at the base of the 5th macrolayer.

The rapid evolution of the mineral chemistry in one cyclic macrolayer may be dependent upon several factors: it may indicate that the crystallizing magma batch had a limited volume and evolved rapidly, because the magma was stratified or because the crystallizing batch was stagnant at the bottom of the chamber and isolated from the main convective magma (Jackson, 1961; Jaupart et al., 1984; Jaupart and Brandeis, 1986). However, zoning in plagioclase and pyroxenes is probably the result of secondary process such as post cumulus overgrowth. But, incomplete reequilibration of Fe-Mg minerals with variable fraction of trapped melt (e.g. Barnes, 1986) and subsolidus reequilibration can also explain their zoning and their compositional trends through the 4th macrolayer.

The cryptic discontinuity between the 4th and 5th macrolayers corresponds to the lithological change. This abrupt change can mark the arrival of more primitive magma by intermittent gravitational instability or perhaps by a new influx in the chamber (Brandeis, 1986; Huppert and Sparks, 1980; Raedeke and McCallum, 1984).

Crystal Size Grading

Crystallinity indexes for plagioclase and pyroxene in cumulates were obtained using Maaloe's counting method (1985), but for surface unity and not for volume unity (see comments of Conrad and Naslund, 1989). The mean sizes of plagioclases and pyroxenes were then calculated

Table 3. Representative chemical analysis of minerals from the 4th macrolayer and the base of the 5th macrolayer. PL: plagioclase; CPX and OPX: Ca-rich and Ca-poor pyroxenes; MGT and ILM.: magnetite and ilmenite. Structural formulas are calculated on the basis of: 8 O for plagioclase; 4 O for olivines; 6 O for pyroxenes; 4 O and 3 cations for magnetites and 3 O and 2 cations for ilmenites. These compositions are used to calculate the fractionation densities of the rocks and of the associations of cumulus minerals.

rock N°	4-A	4-A	4-C	4-G	4-A	4-B	5-A	4-A	4-C	4-G	5-A	4-A	4-C	4-G	5-A	4-A		4-C		5-A	
mineral	PL	PL	PL	PL	olivine	olivine	olivine	CPX	CPX	CPX	CPX	OPX	OPX	OPX	OPX	MGT	ILM	MGT	ILM	MGT	ILM
SiO2	53.76	55.83	55.09	55.49	35.52	35.17	35.76	51.37	49.90	51.61	51.20	53.51	52.57	51.28	52.37	0.00	0.00	0.11	0.04	0.12	0.08
TiO2					0.00	0.00	0.00	0.75	0.36	0.35	0.95	0.19	0.31	0.18	0.29	6.16	52.04	1.04	50.27	12.75	53.27
Al2O3	29.57	28.40	28.69	27.24				2.66	2.11	1.84	2.76	0.98	1.08	0.73	1.16	2.69	0.00	0.27	0.05	2.07	0.00
Fe2O3								0.39	4.76	3.55	1.84	0.00	1.06	2.84	1.68	52.46	2.00	65.15	4.05	40.50	0.38
FeO	0.68	0.11	0.29	0.27	36.98	39.72	38.12	9.47	5.39	6.65	8.98	21.02	23.35	21.87	21.13	36.09	44.99	31.95	43.46	42.90	44.32
MnO					1.02	0.71	0.88	0.33	0.44	0.34	0.34	0.88	0.55	0.62	0.70	0.18	1.68	0.00	1.57	0.53	1.19
MgO					27.00	24.85	26.36	12.76	13.52	13.81	13.68	22.77	21.50	21.22	22.08	0.21	0.00	0.02	0.08	0.00	1.39
NiO					0.00	0.00	0.00														
Cr2O3								0.00	0.08	0.04	0.03	0.00	0.01	0.03	0.00	0.20	0.07	0.80	0.00	0.82	0.00
V2O5																				0.90	0.49
CaO	12.30	10.93	10.78	9.82	0.06	0.01	0.01	21.84	22.13	22.48	21.06	0.71	0.72	0.84	1.29	0.02	0.08	0.02	0.05	0.16	0.00
Na2O	4.23	5.12	5.18	5.88				0.34	0.37	0.35	0.03	0.00	0.00	0.02	0.01						
K2O	0.22	0.22	0.28	0.24																	
Total	100.76	100.61	100.31	98.94	100.52	100.46	101.28	99.91	99.06	100.12	101.15	100.06	101.15	99.63	100.71	98.01	100.87	99.36	99.56	100.79	101.12
Si	2.42	2.50	2.48	2.53	0.99	1.00	0.99	1.93	1.89	1.91	1.90	1.98	1.95	1.94	1.94	0.00	0.00	0.00	0.00	0.00	0.00
Ti					0.00	0.00	0.00	0.02	0.01	0.01	0.03	0.00	0.01	0.00	0.01	0.18	0.98	0.03	0.96	0.36	0.99
Al	1.57	1.50	1.52	1.46				0.12	0.09	0.08	0.01	0.04	0.05	0.03	0.05	12.00	0.00	0.01	0.00	0.09	0.00
Fe3								0.01	0.13	0.10	0.05	0.00	0.03	0.08	0.05	1.52	0.04	1.89	0.08	1.14	0.01
Fe2	0.03	0.00	0.01	0.01	0.86	0.94	0.89	0.30	0.17	0.21	0.28	0.65	0.72	0.69	0.66	1.15	0.94	1.03	0.92	1.34	0.92
Mn					0.02	0.02	0.02	0.01	0.01	0.01	0.01	0.03	0.02	0.02	0.02	0.01	0.04	0.00	0.03	0.02	0.02
Mg					1.12	1.04	1.09	0.71	0.76	0.76	0.76	1.26	1.20	1.20	1.22	0.01	0.00	0.00	0.00	0.00	0.05
Ni					0.00	0.00	0.00														
Cr								0.00	0.01	0.00	0.00	0.00	0.01	0.00	0.00	0.01	0.00	0.02	0.00	0.02	0.00
V																				0.02	0.01
Ca	0.59	0.52	0.52	0.48	0.00	0.00	0.00	0.88	0.90	0.89	0.84	0.03	0.03	0.03	0.05	0.00	0.00	0.00	0.00	0.01	0.00
Na	0.37	0.44	0.45	0.52				0.02	0.03	0.02	0.02	0.00	0.00	0.00	0.00						
K	0.01	0.01	0.02	0.01																	

assuming that crystal sections are squares or circles (Table 4, Figure 5A).

In the 4th macrolayer of ZA2, crystallinity indexes decrease rapidly just above the base, they are fairly constant in the main leucogabbronorite and increase slightly in the reversal for plagioclase, and then return abruptly to a maximum value at the base of the 5th macrolayer. Index variations of plagioclase and clinopyroxene within the unit are quite similar. Calculated mean sizes increase from about 0.3 mm to 1 mm (Figure 5B) for both minerals, which are in the range of the measured sizes. Crystallinity indexes of other macrolayers evolve in the same way, gabbros and norites of the bottom of other units are always fine-grained while leucogabbronorites are coarser-grained.

The crystal-size evolution of clinopyroxene in the 4th macrolayer is not in agreement with Stokes law. The abrupt increase of crystallinity at the base of the macrolayer and its decrease upwards can be linked to many factors including primary processes, such as variation in the kinetics of nucleation and crystal growth (Lofgren, 1974, 1980; Swanson, 1977; Kirkpatrick, 1976; Dowty, 1980; Brandeis et al., 1984; Brandeis and Jaupart, 1987). Reinjection process induce a rapid increase in undercooling of the fresh magma during emplacement. The consecutive change in the thermal regime at the crystallization front is indeed followed by a new burst of nucleation. The accompanying release of latent heat of crystallization minimizes the conductive cooling and the magma undercooling decreases. Crystallization then proceeds under an equilibrium cooling regime, during which crystals reach an "equilibrium size" (nearly constant nucleation rate and crystal growth) of about 1 mm, which is in the range of the most common mineral sizes in layered intrusions (Brandeis, 1986; Brandeis and Jaupart, 1987). The abrupt change in crystallinity between two consecutive macrolayers suggests that the crystallization interval can not adapt progressively to the change in cooling regime, probably because the crystallization interval has been supressed by the magma pulse.

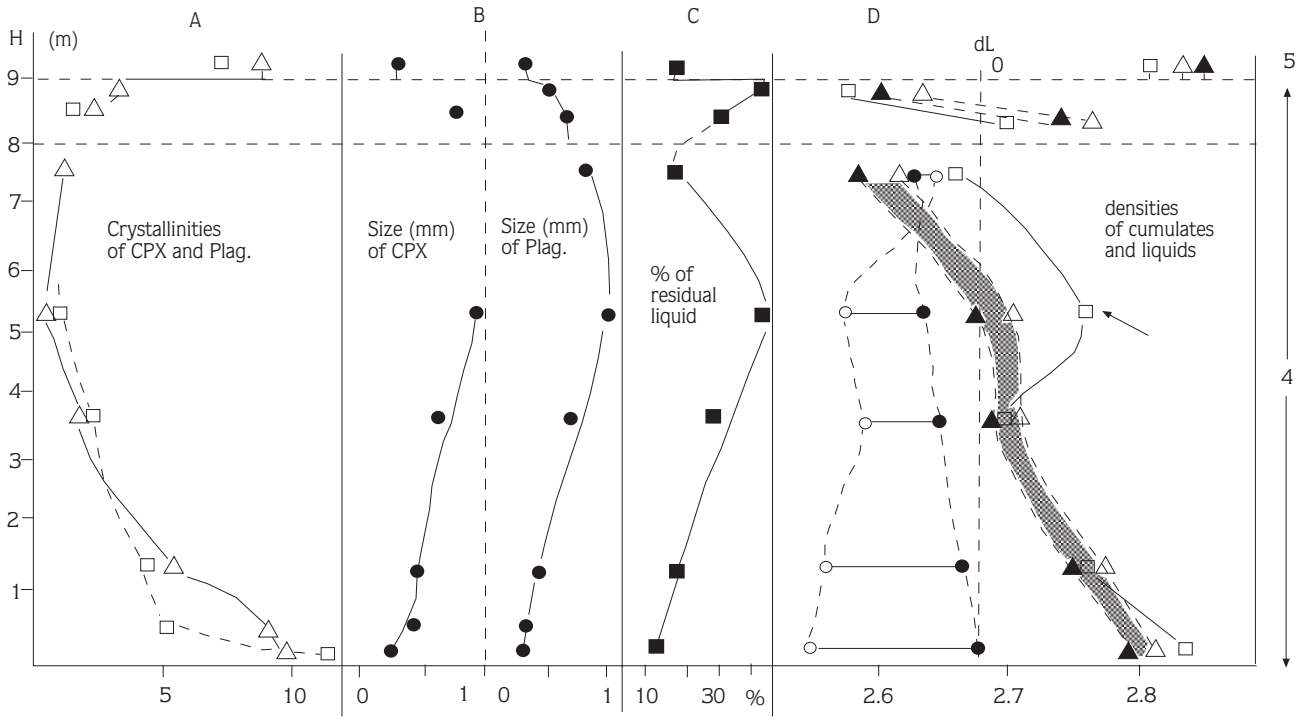

Figure 5. A: Crystallinities for Ca-rich pyroxene (□) and plagioclase (△) through the 4th macrolayer. Crystallinity index C is divided by 100. B: mean calculated crystal sizes. C: estimated percentage of trapped liquid within the successive cumulates. D: fractionation density of cumulus mineral association calculated with, (△) the most Mg-rich mafic phases of each rock type or (▲) the most Mg-rich phases of the macrolayer. □: fractionation density of the whole cumulate (cumulus plus intercumulus phases). ●: density of the parent liquid. ○: density of the residual liquid for an initial porosity $\varnothing_0$ of 0.5. dL_0 : reference density calculated with the composition L'2 corresponding to the 4th macrolayer; arrow: fractionation density of the whole leucogabbronorite (see text).

Table 4. A: Modes of rocks belonging to the 4th unit. See table 2 for rock-types. Mode*: recalculated mode of the cumulus association of each rok. B: Calculated crystallinities and mean crystal size of clinopyroxene and plagioclase (4th unit). N: number of crystals by surface unit; X: mode fraction of the mineral; C: crystallinity. Ø: mean radius of the crystal section considered as a circle. The mean crystal size is Ø= 2√100/C.Π or a = √100/C (mm), according as the crystal section is considered in a first approximation as a circle of radius Ø or a square respectively.

A				4th		macrolayer			5th macrol.
MODE	4-A	4-A'	4-B	4-C	4-D	4-E	4-F	4-G	5-A
Plagioclase	.440	.424	.499	.576	.729	.844	.456	.869	.425
Olivine	.002	.001	.030	.000	.000	.000	.000	.000	.036
Clinopyroxene	.282	.265	.222	.079	.028	.000	.152	.002	.267
Orthopyroxene	.034	.135	.096	.096	.108	.025	.051	.032	.051
Fe Ti oxides	.113	.075	.068	.026	.039	.021	.076	.020	.089
Apatite	.000	.007	.003	.010	.018	.008	.000	.013	.019
Amphibole	.127	.069	.073	.172	.058	.011	.189	.018	.107
Biotite	.001	.012	.006	.038	.019	.089	.019	.033	.002
Chlorite	.001	.006	.001	.001	.001	.001	.056	.009	.001
MODE M*									
Plagioclase*	.525	nd	.595	.724	.789	.964	.624	.944	.502
Olivine*	.002	nd	.037	.000	.000	.000	.000	.000	.046
CPX*	.336	nd	.278	.105	.038	.000	.203	.000	.339
OPX*	.000	nd	.000	.115	.112	.013	.070	.016	.000
Fe Ti oxide*	.135	nd	.085	.039	.031	.013	.101	.016	.088
Apatite*	.000	nd	.004	.015	.030	.010	.000	.019	.024

B		N/cm^2	X	C	Ø (mm)	a (mm)
4-A						
	CPX	360	.282	1276	0.31	0.28
	PL	439	.440	997		0.32
4-A'						
	CPX	134	.265	505	0.50	0.44
	PL	402	.424	948		0.32
C-B						
	CPX	102	.222	459	.52	0.46
	PL	270	.499	541		0.43
4-C						
	CPX	18	.079	228	0.74	0.66
	PL	125	.576	217		0.68
4-D						
	CPX	3	.028	107	1.10	0.96
	PL	77	.729	105		0.97
4-E						
	CPX					
	PL	132	.844	156		0.80
4-F						
	CPX	24	.152	158	0.89	0.79
	PL	11	.456	243		0.64
4-G						
	CPX					
	PL	273	.869	314		0.56
5-A						
	CPX	199	.267	745	0.41	0.36
	PL	363	.425	854		0.34

Coarsening by post cumulus overgrowth or by crystal annealling (Boudreau, 1987; Hunter, 1987, 1996), and resorption of primary phases by reaction with the residual liquid, can, however, strongly alter the primary grain-size gradient related to crytallization kinetics. Coarse hydrous minerals are also more abundant in leucogabbronorites, suggesting that volatile content has affected nucleation and growth rates. Extensive zoning in plagioclases and pyroxenes also suggests that overgrowth of cumulus crytals is effective in the 4th macrolayer. Furthermore, rapid variations of crytal size over distances of two or three metres indicate that the trapped liquid fraction varied rapidely during the macrolayer crystallization.

Modelling of Macrolayer Crystallization

Composition of the Crystallizing Magma

In the absence of chilled margins, it is not easy to approach the composition of the parent magma. However, the lack of peridotite and troctolite, the constant presence of four main phases (Pl, Olv, Opx and Cpx), the olivine substitution by Opx, the presence of quartz in the most evolved rocks, suggest that the parent magma composition was located near the peritectic point of the basaltic system and evolves towards the quaternary minimum.

Major and trace elements of the rocks were determined by X-ray fluorescence analyses of cumulates from the different zones and also throughout the 4th macrolayer of ZA2 (Table 2). The average compositions of the successive zones have been estimated according to mean ratios of rock types within the different zones. Estimates of the volume and mass of the zones were made assuming as a first approximation that their volumes are proportional to their observed thicknesses. One method of calculating the composition of the liquid corresponding to the ZA zone (from L1 to L3, Table 2) of the intrusion is to add the sucessive zone average compositions to the ZC residual zone (residual liquid Lr). However, it is assumed in this type of calculation that magma differentiation acts in a closed system, the reversal at the ZA-ZB boundary implies the opposite,

therefore, the ZB cumulates were not added to the successive ZA subzones.

The first magma L1 corresponding to the base of ZA1 is silica-saturated, Mg and Ni-poor, Al and Fe-rich, it's composition is not so fare from a continental tholeiite. The L2 composition corresponds to the level of the 4th macrolayer. Compared to L1, it is impoverished in Fe, Ti, Mg and Ca, suggesting pyroxene, oxide and plagioclase fractionation (Platevoet, 1990).

Liquidus and solidus temperatures of the magma can be estimated by usual geothermometry methods such as two pyroxene thermometry (Wood and Banno, 1973; Wells, 1977; Lindsley, 1983), and Fe-Ti-oxide thermobarometry (Buddington and Lindsley, 1964; Spenser and Lindsley, 1981). Results (Figure 6) yield minimum equilibrium temperatures ranging from 1100 °C to 700 °C pyroxenes and from 1000 °C to 300 °C for magnetite-ilmenite. The low values are typical for subsolidus mineral reequilibrations. Equilibrium temperatures between plagioclase and liquid (Kudo and Weill, 1971; Mathez, 1973) have also been calculated using microprobe analysis of core plagioclase in leucogabbronorites and the calculated parent liquid composition (Table 1, Figure 6), assuming a total pressure of about 0.2 GPa (the average pressure has been estimated by the method of Carmichael et al., 1970; Nicholls et al., 1971, using Olv-Opx equilibrium and Plag - Ca-Tschermak in Cpx equilibrium). Calculated liquidus temperatures decrease from about 1175±50 °C for the ZA 1 zone to 1100±50 °C for the ZC quartz gabbro.

Amphibole being a post cumulus phase, the near solidus temperatures of the successive liquids can be investigated through the plagioclase-amphibole geothermometer (Blundy and Holland, 1990) obtained for Ti-rich pargasite or hastingsite belonging to ZA and ZB, these high temperatures are confirmed by the high Ti contents of amphiboles (superior to 0.45 Ti cation in the unit-cell) (Helz, 1973).

Magma density and viscosity were calculated for the successive liquid composition, at supposed liquids temperatures by classical methods (Bottinga and Weill, 1970, 1972; Shaw, 1972; Bottinga et al., 1983) (Table 2). Viscosity increases consistently with differentiation and magma density decreases during ZA crystallization.

Trapped Liquid in Cumulates

The abundance of incompatible elements is used to estimate the trapped liquid fraction in cumulates (Henderson, 1968, 1975; Campbell, 1987; Naslund, 1989). The maximum trapped liquid proportion Xi in the cumulates is calculated, assuming that Xi = Csi/Cli, where Csi and Cli are the amounts of a perfectly excluded

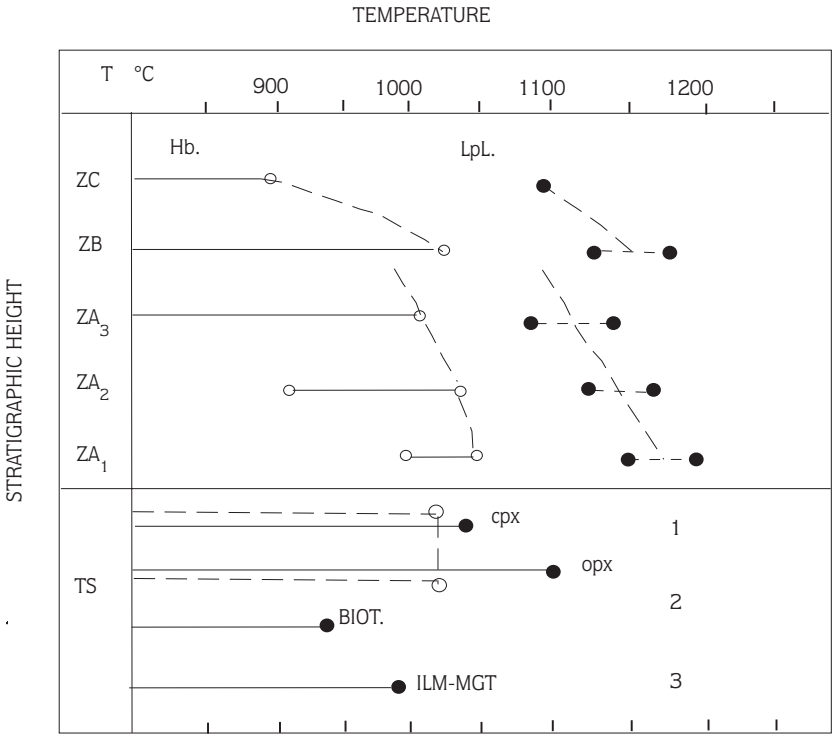

Figure 6. Thermometry based on mineral compositions and parental liquid compositions. L: plagioclase-liquid thermometer. Hb: plagioclase-amphibole thermometer. TS: temperature ranges obtained for the entire series. 1: clinopyroxene-orthopyroxene equilibrium. circles: Wood-Banno and Well's methods; dots: Lindsley's graphical method. 2: temperatures obtained using X_{Mg} of biotite. 3: ilmenite-magnetite equilibrium.

element i in the cumulate and in the corresponding residual liquid, respectively.

In the 4th macrolayer, elements such as Rb and Zr are only used because they seem to be the least compatible elements at the level of ZA2, and because of insufficient analytical accuracy on U, P, Y and REE can not be used as excluded elements because apatite becomes a cumulus phase in ZA2.

In the 4th macrolayer, the trapped liquid fraction (Table 5, Figure 5C) increases rapidly upwards from the base, with more than 40% trapped liquid in leucogabbronorite, but decreases in the first anorthosite (N° 4-E). However, a very high value is found for the second anorthosite (N° 4-G): Rb and Zr are probably not strongly incompatible elements which leads to over-estimate the amount of trapped liquid especially in that rock-type.

Despite these doubts on absolute values, the relative amounts of trapped liquid change within this particular macrolayer and are in good agreement with crystal-size variations. Trapped liquid variations are dependent upon several factors such as the cumulus crystal size (Campbell, 1987), and especially the efficiency with which the residual liquid is expelled throughout the crystallizing cumulate pile, in relation to effects of compaction (Irvine, 1980; McKenzie, 1984) or compositional convection (Huppert ans Sparks, 1980).

Residual Liquid Extraction and Compositional Convection

Density Changes During Crystallization

Density changes during crystallization of the 4th macrolayer of ZA2 can be estimated using the fractionation density parameter introduced by Sparks and Huppert (1984) and knowing the composition of cumulus minerals (by microprobe analyses) and their modal fraction in the cumulus assemblage (the fraction of trapped liquid in cumulates has been estimated above under the subtitle of *Trapped Liquid in Cumulates*). To minimize the effect of mineral reequilibration with trapped liquid (Barnes, 1986), the fractionation density of the successive cumulates is calculated using: Plagioclase core compositions and, (1), the most Mg-rich phases of each rock type; (2), the most Mg-rich phases of the macrolayer; (Table 3).

Assuming an initial porosity $\varnothing_0$ of the cumulate between 0.5 and 0.6, the height Ho of the magma column corresponding to the 4th macrolayer is estimated using the equation:

$$H_0 = [H_c . X_m / (1-\varnothing_0)] . dc / dl_0$$

where X_m is the mean trapped liquid fraction in the 4th macrolayer, Hc the height of the pure cumulate (with 0% trapped liquid), d_c/d_{l0} the ratio between the cumulate and parent liquid densities. The density dlr of the produced residual liquid is given by the formulae of Sparks and Huppert (1984):

$$dl_r = [dl_0 - (1-X_t).DF_c.\bar{V}_c / \bar{V}_0] / (\bar{V}_c/\bar{V}_0) X_i$$

where DF_c is the fractionation density of the pure cumulate c (cumulus phase only), and $\bar{V}c$, $\bar{V}o$ the partial molar volumes. If we consider for simplicity that the difference between $\bar{V}c$ and $\bar{V}o$ is negligible in comparison with the inherent error of the calculation of densities, the formulae becomes:

$$dl_r = [dl_0 - (1-X_i).DF_c] / X_i$$

It is then possible to deduce the height Hr of the residual liquid, which mixes with the parent magma, and the subsequent density change.

The calculations are made from the base to the first anorthosite of the 4th macrolayer and reported in Table 6 and Figure 5D.

The fractionation density of the cumulus assemblage decreases from the gabbroic base to the anorthositic top,

	Rb ppm	Zr ppm	% Liq. (Rb)	% Liq. (Zr)	X (%)
L'2	19	416			
4-A	3.4	115	15	23	15
4-B	4.6	161	20	32	20
4-C	12	166	52	33	33
4-D	11	275	48	54	48
4-E	12	98	52	19	19
4-F	8	226	35	45	35
4-G	13	256	56	51	40
5-A	4.8	154	21	30	21

Table 5. Trapped liquid percentages in the 4th unit (see legend of table 1). It is calculated with the Rb and Zr contents of the successive cumulates. % Liq. (Rb): trapped liquid estimated with Rb. % Liq.(Zr): idem with Zr. X: likely percentage of trapped liquid. L'_2: parental liquid.

A

	C 4-A	C 4-B	C 4-C	C 4-D	C 4-E	C 4-F	C 4-G	C 5-A
SiO2	45.06	47.17	50.31	50.3	52.46	48.64	51.6	46.18
TiO2	2.3	1.78	1.03	0.79	0.31	1.18	0.41	3.22
Al2O3	16.49	18.32	21.75	23.52	28.52	18.22	27.93	15.65
Fe2O3	6.9	4.03	1.81	1.22	0.41	6.33	0.55	2.37
FeO	7.2	6.68	4.91	4.22	1.36	6.22	1.58	8.64
MnO	0.22	0.23	0.18	0.14	0.02	0.17	0.02	0.19
MgO	4.62	4.78	4.04	3.06	0.27	4.25	0.36	5.91
CaO	13.9	13.72	12.14	12.28	12.52	11.36	12.78	14.48
Na2O	2.34	2.72	3.1	3.35	4.07	3.27	3.99	2.42
K2O	0.11	0.13	0.16	0.17	0.21	0.16	0.2	0.1
P2O5	0	0.29	0.62	1.24	0.49	0	0.86	0.99
H2O	0	0	0	0	0	0	0	0
total	99.14	99.75	100.04	100.28	100.64	99.8	100.28	100.15
T°C	1140	1130	1120	1120	1110	1120	1110	1140
density 1	2.82	2.78	2.71	2.71	2.62	2.74	2.64	2.84
	4-A	4-B	4-C	4-D	4-E	4-F	4-G	5-A
T °C	1120	1115	1110	1110	1100	1110	1100	1120
density WR	2.84	2.76	2.7	2.76	2.66	2.7	2.58	2.81

B

N° roche	DFc	Øo	Xi	dlr	Ho (m)	Hc (m)	Hr (m)	dlo
4-A	2.82	0.5	0.15	2.54	9.8	1	0.82	2.68
4-B	2.78	0.5	0.2	2.55	8.67	1.5	1.04	2.66
4-C	2.71	0.5	0.33	2.58	7.02	2	0.8	2.64
4-D	2.7	0.5	0.48	2.57	4.92	1.5	0.11	2.63
4-E	2.62	0.5	0.2	2.64	3.37	2	1.22	2.63

Table 6. A: Fractionation density of the successive cumulates of the 4th unit. C 4-A to C 5-A: compositions of the cumulus assemblages corresponding to the density 1, they are calculated from mineral analyses (see table 3). and corresponding modal (M*) percentage (see table 4). The fractionation densities WR 4 is calculated using the entire rock analyses 4-A to 5-A (see table 2). B: Density evolution of the magma during the crystallization of the 4th macrolayer, calculated from the olivine gabbro 4-A to the anorthosite 4-E. DFc: fractionation density of pure cumulate. Øo: initial porosity. Xi: calculated fraction of trapped liquid. dlr: density of the produced residual liquid. Ho: initial height of magma. Hc: height of the cumulate. Hr: height of the expelled residual liquid. dlo: density of the successive parent liquid, the first liquid is L'2 (table 2).

in conformity with plagioclase enrichment. As a result, the residual liquid is first lighter than the parent liquid, but it becomes denser at the level of anorthosite.

As crystallization proceeds, the density contrast between the parent magma 1_0 and the produced residual liquid 1_r decreases. Subsequenty, the residual liquid extraction, at the nucleation front, becomes less and less efficient.

The convective velocity and crystallization velocity

The convective velocity Vc at the crystallization front is calculated using the formulation of Sparks et al (1985):

$V_c=(D^2.g.\Delta d.\ \varnothing^{4.5}) / 10\mu$

Using a density contrast Δd of 0.15, a mean crystal-size D between 0.25mm and 0.30mm and the initial porosity $\varnothing_0$, V_c reaches a maximum of 30cm/year during the crystallization of the macrolayer base. The convective velocity drops to 10cm/year during the crystallization of the leucogabbronorite, in which the estimated trapped liquid fraction is important.

The minimum value of V_c also gives a time-scale for the crystallization of the cumulates. If one takes an elementary cumulate layer with a thickness in the same order as the mean diameter of crystals (0.3mm at the base), it takes about one day to obtain crystals of 0.3mm. If crystallization is an uninterrupted process in the chamber, it takes about 10.000 years to form the 1.000m thick pile of cumulates.

Anorthosite formation at the top of a macrolayer

The residual liquid became denser than the parent liquid during leucogabbronorite to anorthosite

crystallization (Figure 5D). A strongly unstable density gradient was created and might instigate intercumulus compostional convection in the cumulate pile. The great increase of the fractionation density of the whole leucogabbronorite (cumulus plus intercumulus phases; shown by an arrow on Figure 5D) compared to DFc of the corresponding pure cumulate, suggest that a dense residual liquid has sunk through the cumulate pile.

One of the important features of the layering is that, at the top of the macrolayer, there is a crystallization sequence ranging from multiphase cumulates to single phase cumulates (anorthosite). This apparently non-cotectic crystallization behaviour of the magma could be linked to the migration of dense residual liquid which is replaced by a lighter liquid coming from the underlying leucogabbronorite and/or from the overlying magma. The renewal of intercumulus liquid could induce adcumulus growth of plagioclase only, while the associated mafic cumulus phases rather are dissolved, leading finally to anorthosite formation at the top of the crytallizing layer, this process was also proposed by Boudreau and McCallum (1992) for the Stilwater intrusion, and had been also debated by Mc Birney (1995) for the Skaergaard intrusion.

Many processes have been invoked to explain adcumulate growth of crystals: chemical diffusion at the crystallization interface (Hess, 1960; Wager, 1960; Wadswoorth, 1985), nucleation and growth rates which control the primary cumulate porosity (Campbell, 1987), compaction and infiltration metasomatism (Irvine, 1980; McKenzie, 1984), intercumulus compositional convection (Tait et al., 1984; Sparks et al., 1985). All these processes can act in different ways, according to each situation, to each reservoir-type. Here, compaction and infiltration metasomatism were probably of little importance, because the modal contact between the 4th and 5th macrolayers of ZA2 coincides wit changes in mineral compositions. However, detailed studies of more macrolayers are needed to know the exact role of infiltration metasomatism compared with intercumulus compositional convection, in the formation of anorthosite at the top of the macrolayers.

Crystallization Processes in a Small Chamber Compared with Other Chambers

In-situ Crystallization

In the Peloso complex, the *in-situ* crystallization of one single macrolayer such as the 4th macrolayer studied in this paper, can take place at the bottom of a ten to twenty metres thick magma layer, at the temporary chamber floor.

Within the crystallizing zone, the convective velocity was at a maximum in the first formed metres of cumulates, because the density of the cumulate is high compared with the hypot et hical parent liquid, and a light residual liquid could be efficiently extracted from the cumulate pile and be mixed with the overlying magma layer.

The density of the residual liquid increases with increasing amounts of plagioclase in the cumulus assemblage. When leucogabbronorites crystallize, the volume of liquid expelled at the crystallization front is not very important, leading to orthocumulate formation. These orthocumulates represent the major part of the cumulates of the Peloso complex. The lack of adcumulates and the strong prevalence of orthocumulates in the Peloso intrusion, means that the convective velocity was never very much higher than the crystallization velocity, but that their ratio was not constant during a complete macrolayer crystallization. This always leads to a final residual porosity higher than 0.1 (Sparks et al., 1985; Kerr and Tait, 1986), which corresponds to the estimated trapped liquid fraction in gabbro at the bottom of the macrolayer. The apparent lack of compaction can be the result of solidification and convective velocities which were too high relative to the compaction rate (Sparks et al., 1985) for a 1 km thick body, such as the Peloso intrusion. This is quite different for large magmatic chambers where important volume of adcumulate are often observed, and where the crystallization front velocity is very slow compared to the convective velocity of residual melts.

The minimum convective velocity also gives the rate of macrolayer crystallization, about 10cm/year, and the 1.000m thick observed sequence could represent about 10.000 years of magmatic activity.

Removal of Magma and Reinjection Process

The intermittent removal of magma at the floor is achieved by two possible processes. With time, the remaining batch of magma becomes less dence than the overlying (stratified?) magma and could be periodically removed by gravitative instability. New influx of primitive magma may also cause the removal of magma at the crystallization front (Huppert and Sparks, 1980; Raedeke and McCallum, 1984).

Intermittent influxes of primitive magma is well supported by the isotopic evolution throughout the cumulate pile (Figure 7). Decreasing Sr_i initial ratio and increasing εNd_i show that the more primitive magmas are also the more contaminated (Poitrasson et al., 1994). In other terms, the crystallization history of the chamber is

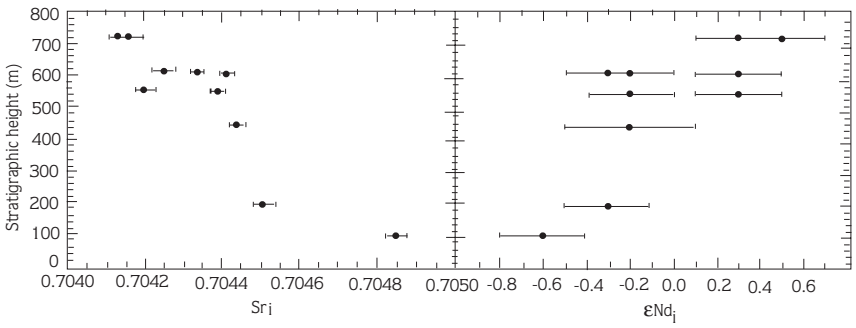

Figure 7. Sri and εNdi evolutions versus stratigraphic height in the ZA part of the Peloso layered complex (data after Poitrasson et al., 1994).

dominated by the RFC process, whereas the AFC process is apparently dominant in large magma bodies such as in the Skaergaard intrusion (Stewart and De Paolo, 1990).

Crystal Size Grading in Cumulates

In the Peloso intrusion, the grain-size evolution throughout a single macrolayer, the fraction of trapped liquid in the successive cumulates and the fractionation density of the cumulus association are linked. If the primary crystal-size are dependent upon the kinetics of nucleation and crystal growth, the final crystal-sizes are strongly dependent upon the intensity of residual melt extraction by compositional convection.

In a sequence of cumulate where the modal variations are important, the final crystal-size of cumulates are dependent upon:

(i), specific adcumulus growth at the crystallization front or during the densification of the cumulate (R.H. Hunter, 1996);

(ii), partial resorption of primary phases by reaction with liquids migrating through the cumulate;

(iii), post-cumulus textural reequilibration of crystals (named also annealling of crystals).

Therefore, there is little propability that final crystal-size variations in cumulates would still be directly related to initial crystallization kinetics (at the liquidus), in particular, within large reservoir where cooling and crystallization history is long, but also in small reservoirs where the crystallization velocity and the convective velocity are not very different, leading to an important trapped liquid fraction in cumulates.

References

Baker, B.H. and McBirney, A.R., 1985, Liquid fractionation III: geochemistry of zoned magmas and the compositional effects of liquid fractionation. J. Volcanol. Geotherm. Res., 24, 55-81.

Barnes, S.J., 1986, The effects of trapped liquid crystallization on cumulus mineral compositions in layered intrusions. Contrib. Mineral. Petrol., 93, 524-531.

Blundy, J.D., and Holland, T.J., 1990, Calcic amphibole equilibria and a new amphibole plagioclase geothermometer. Contrib. Mineral. Petrol., 104, 208-224.

Bonin, B., 1972, Le complexe granitique subvolcanique de la region de Tolla-Cauro, Corse. These de 3e cycle, University og Paris VI, publ. No: 7, E.N.S. Paris, 127 pp.

Bonin, B., 1980, Les complexes acides alcalines continentaux: 1'exemple de la Corsa. Thése d'état, University of Paris VI, 650pp.

Bottinga, Y., and Weill, D.F., 1970, Densities of liquid silicate systems calculated from partial molar voumes of oxide components. Amer J. Sci., 269, 169-182.

Bottinga, Y., and Weill, D.F., 1972, The viscosity of magmatic silicate liquids: a model for calculation. Amer. J. Sci., 272, 438-475.

Bottinga, Y., Richet, P., and Weill, D.F., 1983, Calculation of the density and thermal expansion coefficient of silicate liquids. Bull. Mineral., 106, 129-138.

Boudreau, A.E., 1987, Pattern formation during crystallization and the formation of fine scale layering. In: Origins of Igneous Layering, Parsons, I., (ed), 453-471, D. Reidel Publ. Co.

Boudreau, A.E. and McCallum I.S., 1992, Infiltration metasomatism in layered intrusions-An example from the Stillwater Complex, Montana. J. Volc. Geotherm. Res., 52, 171-183.

Brandeis, G., Jaupart, C., and Allegre, C.J., 1984, Nucleation, crystal growth and thermal regime of cooling magmas. J. Geophys. Res., 89, 10161-10177.

Brandeis, G., 1986, Modéles physiques de convection et crystallisation dans les chambres magmatiques. Thése d'état, University of Paris VII, 389pp.

Brandeis, G., and Jaupart, C., 1987a, The kinetics of nucleation and crystal growth and scaling laws for magmatic crystallization. Contrib. Mineral. Petrol., 96, 24-34.

Brandeis, G., and Jaupart, C., 1987b, Crystal sizes in intrusions of different dimensions: constraints on the cooling regime and the crystallization kinetics. In: Magmatic Processes, physicochemical principles. B.O. Mysen (ed), Geochemical Soc. Spec. Pupl. 1, 307-318.

Buddington, A.F., and Lindsley, D.H., 1964, Iron titanium oxide minerals and synthetic equivalents. J. Petrology, 5, 310-357.

Campbell, I. H. 1978, Some problems with the cumulus theory. Lithos, 11, 311-323.

Campbell, I. H. 1987, Distribution of orthocumulate textures in the Jimberlana intrusion. J. Geology, 95, 35-54.

Carmichael, I.S.E., Nicholls, J., and Smith, A.L., 1970, Silica activity and P total in igneous rocks. Amer. Mineral., 55, 246-263.

Chen, C.F. and Turner, J.S., 1980, Crystallization in double diffusive system. J. Geophys. Res., 85, 2573-2593.

Conrad, M.E., and Naslund, H.R., 1989, Modally graded rhythmic layering in the Skaergaard intrusion. J. Petrology, 30, 251-269.

Dowty, E., 1980, Crystal growth and nucleation theory and the numerical simulation of igneous

crystallization. In: Physics of Magmatic Processes, Princeton University Press, 419-485.

Helz, R.T., 1973, Phase relations of basalts in their melting ranges at PH2O= 5Kb, as a function of oxygen fugacity. I: mafic phases. J. Petrology, 14, 249-302.

Henderson, P., 1968, The distribution of phosphorus in the early and middle stages of fractionation of some basic layered intrusions. Geochim. Cosmochim. Acta, 32, 897-911.

Henderson, P., 1975, Geochemical indicator of the efficiency of fractionation of the Skaergaard intrusion, East Greenland. Mineral. Mag., 40, 286-291.

Hess, H.H., 1960, Stillwater igneous complex, Montana, a quantitative mineralogical study. Goel. Soc. Amer. Mem., 80, 1-230.

Hunter, R.H., 1987, Textural equilibrium in layered igneous rock. In: Origins og Igneous Layering, Parsons, I., (Ed), 473-503, D. Reidel Publ. Co.

Hunter, R.H., 1996, Texture development in cumulate rocks. In: Layered Intrusion, Cawthorn, R.G., (ed.), Developments in Petrology 15, Elsevier Science publ., 530 pp.

Huppert, H.E., and Sparks, R.S.J.,1980, The fluid dynamics of a basaltic magma chamber replenished by an influx of hot, dense, ultramafic magma . Contrib. Mineral. Petrol., 75, 279-289.

Huppert, H.E., Sparks, R.S.J., Wilson, J.R., and Hallworth, M.A., 1986, Cooling and crystallization at an inclined plane. Earth Planet. Sci. Lett., 79, 319-328.

Irvine, T.N., 1974, Petrology of the Duke Island ultramafic complex, Southeasthern Alaska. Geol. Soc. Amer. Mem., 138.

Irvine, T.N., 1980, Magmatic infiltration metasomatism, double diffusive fractional crystallization and adcumulus growth in the Musko and other layered intrusions. In: Physics of Magmatic Processes, Princeton University Press, 325-383.

Irvine, T.N., 1982, Terminology for layered intrusions. J. Petrology, 23, 127-162.

Irvine, T.N., Keith, D.W., and Todd, 1983, The J.M. Platinium Palladium Reef of the Stillwater complex, Montana. II: origin by double-diffusive convective magma mixing and implications for the Bushveld complex. Econ. Geol., 78, 1287-1334.

Irvine, T.N., 1987, Processes involved in the formation and development of layered igneous rocks. In: Origins of Igneous Layering, Parsons, I., (Ed.), NATO ASI Series, 196, 649-656.

Jackson, E.D., 1961, Primary textures and mineral associations in the ultramafic zone of the Stillwater complex, Montana. US Geol. Survey Prof. Paper, 358, 106.

Jaupart, C., Brandeis, G., and Allegre C.J., 1984, Stagnant layers at the bottom of convecting magma chambers. Nature, 308, 535-538.

Jaupart, C. And Brandeis, G., 1986, The stagnant bottom layer of convecting magma chambers. Earth Planet. Sci. Lett., 80, 183-199.

Kerr, R.C., and Tait, S.R., 1986, Crystallization and compositional convection in a porous medium cooled from below with application to layered igneous intrusions. J. Geophys Res., 91, 3591-3608.

Kirkpatrick, R.J., 1976, Towards a kinetic model for the crystallization of magma bodies. J. Geophys. Res., 81, 2565-2571.

Kudo, A.M. and Weill, D.F., 1970, An igneous plagioclase thermometer. Contrib. Mineral. Petrol., 25, 52-65.

Lindsley, D.H., 1983, Pyroxene thermometry. Amer. Mineral., 68, 477-493

Lofgren, G., 1974, An experimental study of plagioclase crystal morphology, isothermal crystallization. Am. J. Sci., 274, 243-273

Lofgren, G., 1980, Experimental studies on the dynamic crystallization of silicate melts: In: Physics of Magmatic Processes. Princeton University Press, 487-551

Maaloe, S., 1978, The origin of rhythmic layering. Mineral. Mag., 42, 337-345

Maaloe, S., 1985, Igneous petrology. Berlin, Springer-Verlag, 374 pp.

Marsh, B.D., 1989a, On convective style and vigor in sheet-like magma chambers. J. Petrol., 30, 479-530

Marsh, B.D., 1989b, Magma chambers. Ann. Rev. Earth Planet. Sci. Lett., 17, 439-474

Mathez, E.A., 1973, Refinement of the Kudo-Weill plagioclase thermometer and its application to basaltic rocks. Contrib. Mineral. Petrol., 41, 61-72.

McBirney, A.R., 1995, Mechanism of differentiation in the Skaergaard Intusion. J. of the Geol. Soc. London, 152, 421-435.

McBirney, A.R. and Noyes, R., 1979, Crystallization and layering of the Skaergaard intrusion. J. Petrology, 25, 185-212.

McKenzie, D.P., 1984, The generation and compaction of partially molten rock. J. Petrology, 25, 713-765.

Naslund, H.R., 1989, Petrology of the Basistoppen Sill, East Greeland: a calculated magma differentiation trend. J. Petrology, 30, 2, 299-319.

Nicholls, J., Carmichael, I.S.J., and Stormer, J.C., 1971, Silica activity and P total in igneous rocks. Contrib. Mineral. Petrol., 33, 1-20

Parsons, I., 1987, Origins of igneous layering. NATO ASI series, 196, 666 pp.

Platevoet, B., 1985, Le massif alcalin du Peloso (Corse): un complexe lité associé ‡ des monzosyénites. C.R. Acad. Sci. Paris, 301, 6, 787-790.

Platevoet, B., 1990, Le plutonisme basique et intermédiaire dans le magmatisme anorogénique de Corse. Thése d'état, University of Paris-Sud, 510 pp.

Poitrasson, F., Pin,Ch., Duthou, J.L. and Platevoet, B., 1994, The size-isotopic evolution connection among layered mafic intrusions: clues from a Sr-Nd isotopic study of a small complex. J.G.R. 99, B5, 9441-9451.

Raedeke, L.D. and McCallum, I.S., 1984, Investigations in the Stillwater complex, part II: Petrology and petrogenesis of the ultramafic series. J. Petrology, 25, 395-420.

Shaw, H.R., 1972, Viscosities of magmatic silicate liquids: an empirical method of prediction. Amer. J. Sci., 272, 870-893.

Sparks, R.S.J. and Huppert, H.E., 1984, Density changes during the fractional crystallization of basaltic magmas: fluid dynamic implications. Contrib. Mineral. Petrol., 85, 300-309.

Sparks, R.S.J., Huppert, H.E., Kerr, R.C., McKenzie, D.P. and Tait, S.R., 1985, Postcumulus processes in layered intrusions. Geol. Mag., 122, 555-568.

Spencer, K.J. and Lindsley, D.H., 1981, A solution model for coexisting iron-titanium oxides. Amer. Mineral., 66, 1189-1201.

Swanson, S.E., 1977, Relation of nucleation and crystal growth rate to the development of granitic textures. Amer. Mineral., 62, 966-976.

Tait, S.R., Huppert, H.E. and Sparks, R.S.J., 1984, The role of compositional convection in the formation of adcumulate rockas. Lithos, 17, 139-146.

Vellutini, J., 1977, Le magmatisme Permien du Nord-Ouest de la Corse, son extention en Méditerranée Occidentale. Thése d'état, University of Marsielle, 276 pp.

Wadsworth, W.J., 1985, Terminology of postcumulus processes and products in the Rhum layered intrusion. Geol. Mag., 122, 549-554.

Wager, L.R., 1960, Differing powers of crystal nucleation as a factor for producing diversity in layered igneous intrusions. Geol. Mag., 96, 75-80.

Wager, L.R., and Brown, G.M., 1968, Layered igneous rocks. Edinburgh and London, Oliver and Boyd Ltd., 588 pp.

Wells, P.R.A., 1977, Pyroxene thermometry in simple and complex systems. Contrib. Mineral. Petrol., 62, 129-139.

Wilson, J.R., and Larsen, S.B., 1985, Two dimensional study of a layered intrusion: the Hyllingen series, Norway. Geol. Mag., 122, 97-124.

Wood, B.J., and Banno, S., 1973, Garnet-orthopyroxene and orthopyroxene-clinopyroxene relationships in simple and complex systems. Contrib. Mineral. Petrol., 42, 109-124.